Atmospheric
Chemistry
and Physics
Discussions

Ozone production
and trace gas
correlations

H. Fischer et al.

Title Page

Abstract	Introduction
Conclusions	References
Tables	Figures

I◀	▶I
◀	▶
Back	Close

Full Screen / Esc

Print Version

Interactive Discussion

© EGU 2002

Ozone production and trace gas correlations during the June 2000 MINATROC intensive measurement campaign at Mt. Cimone

H. Fischer[1], R. Kormann[1], T. Klüpfel[1], Ch. Gurk[1], R. Königstedt[1], U. Parchatka[1], J. Mühle[1], T. S. Rhee[1], C. A. M. Brenninkmeijer[1], P. Bonasoni[2], and A. Stohl[3]

[1]Max Planck Institute for Chemistry, POB 3060, 55020 Mainz, Germany
[2]National Research Council, Institue of Atmospheric Sciences and Climate, via Gobetti 101, 40129 Bologna, Italy
[3]Technical University of Munich, Chair of Bioclimatology and Air Pollution Research, Am Hochanger 13, 85354 Freising-Weihenstephan, Germany

Correspondence to: H. Fischer (hofi@mpch-mainz.mpg.de)

Ozone production and trace gas correlations

H. Fischer et al.

© EGU 2002

Abstract

An intensive measurement campaign was performed in June 2000 at the Mt. Cimone station ($44°\,11'$ N – $10°\,42'$ E, 2165 m asl, the highest mountain in the northern Italian Apennines) to study photochemical ozone production in the lower free troposphere. In general, average mixing ratios of important trace gases were not very high (121 ± 20 ppbv CO, 0.284 ± 0.220 ppbv NO_x, 1.15 ± 0.8 ppbv NO_y, 58 ± 9 ppbv O_3), which indicates a small contribution by local pollution. This is supported by the analysis of volatile organic compounds (VOCs), that exhibit mean levels typical for background continental air (e.g. 905 ± 200 pptv C_2H_6, 268 ± 110 pptv C_3H_8, 201 ± 102 pptv C_2H_2, 111 ± 124 pptv isoprene, 65 ± 33 pptv benzene). Furthermore, significant diurnal variations for a number of trace gases (O_3, CO, NO_x, NO_y, HCHO) indicate the presence of free tropospheric airmasses at nighttime as a consequence of local catabatic winds. Average mid-day peroxy radical concentrations at Mt. Cimone are of the order of 30 pptv. At mean NO concentrations of the order of 40 pptv this gives rise to significant in situ net O_3 production of 0.1–0.3 ppbv/hr. The importance of O_3 production is supported by correlations between O_3, CO, NO_z, and HCHO, and between HCHO, CO and NO_y.

1. Introduction

Ozone in the troposphere originates either from the stratosphere by downward transport to the troposphere at extra-tropical latitudes, often in connection with tropopause folding events (e.g. Holton et al., 1995 and references therein), or from in situ photochemical production involving NO_x, CO, and hydrocarbons (e.g. Crutzen, 1995). In rural and remote environments an important fraction of the tropospheric ozone is due to in situ photochemical production. It is well established by model studies and observations that ozone production in remote areas is usually limited by the availability of NO_x. Photochemical ozone production has been studied extensively in rural environments (see Kleinman, 2000; Trainer et al., 2000 for recent reviews of observation-based anal-

Title Page

Abstract	Introduction
Conclusions	References
Tables	Figures

⏮   ⏭

◀   ▶

Back   Close

Full Screen / Esc

Print Version

Interactive Discussion

© EGU 2002

ysis of ozone production in rural environments), while studies in the remote troposphere are less common (Ridley and Robinson, 1992; Atlas and Ridley, 1996; Fischer et al., 1998; Zanis et al., 2000a, b). Often, free tropospheric measurements are obtained from airborne investigations, which place limitations on the number of species that can be measured and on their temporal coverage. As an alternative, high-altitude measurements at mountainous sites can be used to yield information on the free troposphere, provided that local orographic influences can be quantified.

To determine the net ozone production and the oxidizing power of the free troposphere, accurate measurements of the photolysis frequencies of O_3 and NO_2, as well as sensitive measurements of the concentrations of NO, NO_2, O_3, RO_x, CO, and VOCs have to be made. In addition, measurements of formaldehyde (HCHO), an intermediate species originating from the photochemical degradation of CH_4 and NMVOCs (non-methane volatile organic compounds), can be used to gain information about the level of chemical activity (Wagner et al., 2002). In June 2000 an intensive measurement campaign was performed at Mt. Cimone (44° 11′ N, 10° 42′ E, 2165 m asl) (Bonasoni et al., 2000) to study ozone formation in the free troposphere over this part of continental Europe. Accurate measurements of NO, NO_2, HNO_3, NO_y (sum of reactive nitrogen species), O_3, HCHO, CO, CH_4, NMVOCs, HO_2, RO_2, O_3 photolysis frequency, aerosol and meteorological parameters were performed by a consortium of European institutes in the framework of MINATROC (MINeral dust And TROpospheric Chemistry). An overview of the goals of MINATROC in general and the Mt. Cimone experiment in particular can be found in Balkanski et al. (this issue).

2.   Trace gas measurements at Mt. Cimone

The instrumentation operated by the Max Planck Institute for Chemistry was housed in a laboratory building while air sampling was accomplished at a height of 8 m above the roof of the building using a telescopic mast. The air was transferred to the instruments using 1/4" OD PFA tubing wrapped in black sealing to avoid photochemical

Ozone production and trace gas correlations

H. Fischer et al.

decomposition of photolabile species inside the sampling lines.

A Tunable Diode Laser Absorption Spectroscopy (TDLAS) instrument was used for the measurement of NO_2, HCHO, and H_2O_2. The TDLAS is described in detail in (Wienhold et al., 1998; Kormann et al., 2002). Absorption lines at $1608.1\,cm^{-1}$ (anti-symmetric streching vibration), $1760.9\,cm^{-1}$ (C-O stretching vibration) and $1248.0\,cm^{-1}$ (O-H bending vibration) were used for NO_2, HCHO and H_2O_2, respectively. The time resolution of the original data is 90 s. In situ calibrations were performed every 15 min by replacing ambient air with known amounts of calibration gas standards (permeation devices) while zero gas measurements were made every 90 s, applying scrubbed ambient air to the inlet (Kormann et al., 2002). The uncertainty of the calibration gas standards was estimated to be of the order of 10%. The precision, deduced from the reproduceability of the in-field calibrations was 1.9% (NO_2) and 2.6% (HCHO), while the detection limit according to the reproduceability of the zero air measurements was 46 pptv (NO_2) and 102 pptv (HCHO) for the 90 s time resolution. Post campaign averaging of the data over 30 min further improved the precision and detection limit of those measurements. Reliable data for H_2O_2 could not be gained due to a technical problem with the laser diode used for this species.

Total reactive nitrogen (NO_y) was measured after conversion to NO in a heated Au-converter in the presence of CO using a chemiluminescence detector (Tecan CLD 770 ppt). The Au-converter was mounted on top of the sample mast thus avoiding the need for an additional inlet line (Lange et al., 2002). Zero and calibration gas (NO, NO_2) were added to the converter every 15 min. The time resolution was 10 s, the accuracy was about 22%, the precision was 14% and the noise level was 90 pptv. A second CLD was used for NO measurements (time resolution 10 s, accuracy 5%, precision 2.2%, detection limit 3.5 pptv).

CO was measured every 4 min using an in situ gas chromatograph with a gas reduction (HgO) detector (GC/HgO). The instrument was calibrated every 6 hr using two NOAA traceable secondary standards (accuracy 4.2%) with a reproduceability of 1.5%.

A peroxy radical chemical amplifier (PERCA), based on the design of Hastie et

al. (1991), was used for the measurement of peroxy radicals (RO_x). The instrument is placed in a small refrigerator regulated to 280 K (Perner et al., 1999) mounted on top of the laboratory building (1.5 m above the roof). The chain length of the radical amplifier was determined three times during the campaign using the photolysis of H_2O as a source of HO_2 radicals (Schultz et al., 1995). As shown by Mihele and Hastie (1998), the chain length of a PERCA is sensitive to the concentration of ambient water. Therefore, the chain length was determined in the laboratory as a function of the water vapor concentration, and the field data were corrected after the campaign based on measurements of the relative humidity. The detection limit of the PERCA used is better than 7 pptv (typically 2 pptv @ 1 min time resolution), the noise level (1 min time resolution) is 8–10 pptv, and the accuracy is 40–60%. Note that additional measurements of HO_2 and RO_2 were made by the Max Planck Institute for Nuclear Research in Heidelberg using the ROXMAS technique. Details of these measurements and a comparison of the total RO_x levels measured by the two instruments can be found in Uecker et al. (2001) and Hanke et al. (2002).

Ozone mixing ratios were determined every 60 s from UV absorption measurements (Ansyco 41 M) with an accuracy better than 5%, while the ozone photolysis rate ($J(O^1D)$) was measured using two filter radiometers (Meteorology Consult), measuring the up- and downward flux of radiation in the UV-B range with a total uncertainty of 20–50% depending on solar zenith angle. An additional ozone measurement was performed at the station by CNR-ISAO (UV-Absorption Dasibi, inlet ~ 8 m above the ground). A linear regression analysis yielded O_3 (CNR-ISAO) = 0.89 O_3 (MPI-C) + 8, $R^2 = 0.82$, indicating a tendency for higher O_3 concentrations obtained by the MPI-C instrument. Since an in-field comparison of the calibration standards was not performed, this discrepancy remains unresolved.

In addition to these in situ measurements, 26 stainless steel electropolished canisters were filled for post-campaign analysis of volatile organic compound (VOC) (ethane, ethene, propane, propene, isobutane, butane, acetylene, trans-2-butene, 1-butene, cis-2-butene, 2-methylbutane, pentane, cyclohexane, 2-methylpentane, 3-methylpentane,

hexane, isoprene, benzene) and for greenhouse gases (sulfur hexafluoride, carbon dioxide, methane, nitrous oxide). The VOC analysis was made in the home laboratory using gas chromatography with mass spectrometric detection (GC/MS) (Mühle et al., 2002). The 26 samples were separated on a 50 m, 0.32 mm ID, 5 μm Al$_2$O$_3$/KCl

5 porous layer open tubular (PLOT) column (Chrompack) by using a gas chromatograph (Hewlett-Packard, HP 6890) connected to a quadrupole mass spectrometer (HP 5973). A 30 compound reference standard from the National Physical Laboratory (Teddington, UK) with a certified uncertainty range of 1.2 to 2.2% (95% confidence limit) for each compound was used for absolute calibration. The detection limits (3σ variation of a

10 blank sample) were 1 to 7.4 pptv (alkanes), 0.3 to 2.7 pptv (alkenes) and 8 pptv (acetylene, benzene) and the precision is 1 to 15%.

Additional measurements of meteorological parameters (T, p, RH, wind speed and direction) were made by CNR-ISAO. For the following data analysis, a merged data set based on 30 min averages of the in situ data has been used.

15 **3. Results and discussion**

3.1. Data overview

Near-continuous, 24-hour measurements were made during the intensive measurement period between 1–30 June, with the exception of CO, which was measured only after 14 June. Canister samples were taken on 6 June (2 samples), 7 June (2 samples),

20 9 June (3 samples), 10 June (1 sample), 14 June (3 samples), 15 June (1 sample), 19 June (2 samples), 27 June (1 sample), 28 June (1 sample), 29 June (1 sample), 2 July (1 sample), 3 July (3 samples), and 4 July (4 samples). Figure 1 shows the time series for J(O^{1}D), RO$_x$, HCHO, O$_3$, CO, NO$_x$ (NO + NO$_2$), NO$_y$, RH, p, T, and the airmass origin deduced from back-trajectories. A statistical analysis of the trace gas measure-

25 ments for the complete data set, and subdivisions into daytime (06:00–20:00 GMT) and nighttime (20:00–06:00 GMT) observations is given in Table 1. In general, the trace gas

levels are relatively low, indicating that the site is not significantly affected by local pollution. Daytime median levels of O_3, CO, NO_x, NO_y and HCHO are 56 ppbv, 119 ppbv, 0.267 ppbv, 0.897 ppbv and 1.4 ppbv, respectively. Median concentrations of RO_x are of the order of 17 pptv. In particular, the low levels of NO_x, NO_y and the ratio NO_x/NO_y

5 ~ 0.3 confirm that photochemically aged airmasses are probed at the site. This is further supported by the relatively low levels of NMHC (Table 2). During the night, slightly higher median levels are observed for O_3 (60 ppbv) and NO_y (1.027 ppbv), while lower levels are found for NO_x (0.197) and HCHO (1.107 ppbv), as compared to daytime conditions. Peroxy radical levels are generally below the detection limit during the night.

10 Lowest levels for NO_x, NO_y, CO and HCHO were observed during the nights of 5/6, 19/20, 20/21, 21/22, and 22/23 June. During these nights the relative humidity dropped to values below 40%, while the wind speed generally exceeded 5 m/s, thus indicating downward transport of air from the free troposphere. This is reflected in the average trace gas levels, which are 78 ± 53 pptv for NO_x, 254 ± 180 pptv for NO_y, 56 ± 8 ppbv

15 for O_3, 100 ± 8 ppbv for CO and 334 ± 128 pptv for HCHO. Additional measurements of low concentrations of cloud condensation nuclei (CCN) (van Dingenen et al., this issue), as well as enhanced CO_2 concentrations (Bonasoni et al., this issue) further support the interpretation that the airmasses originated from the free troposphere (note that in summer CO_2 concentrations in the continental boundary layer are generally

20 lower than free tropospheric concentrations due to uptake by vegetation; Fischer et al., 2002).

The highest trace gas levels were observed in the late afternoon of 9 June, between 18:00 and 23:00 GMT during easterly to south-easterly flow. During this period NO_x and NO_y increased to 2.2 and 5 ppbv, respectively, while maximum HCHO values of

25 nearly 5 ppbv were measured. Unfortunately CO was not measured during this first phase of the campaign, but very high concentrations of CCN of the order of $1.3 -$ 1.4×10^5 (van Dingenen et al., this issue) and highly elevated O_3 concentrations of more than 100 ppbv indicate that most probably photochemically processed polluted boundary layer air masses reached the site.

The lower panel of Fig. 1 documents an airmass classification deduced from 144 h (6 days) three-dimensional back-trajectories calculated every 3 h with the FLEXTRA trajectory model (Stohl et al., 1995). The classification is based on the geographical region over which the airmasses spent most of their time before reaching Mt. Cimone (Balkansky et al., this issue; van Dingenen et al., this issue), leading to a subdivision into 6 classes: Arctic (ARC), North-Western Europe (NWEU), Western Europe (WEU), Eastern Europe (EEU), the Mediterranean Basin (MED) and the Saharan-African (AFR) area). Table 3 shows trace gas levels (mean $\pm 1\sigma$-standard deviation calculated for a 3 h period centered around the time of the back-trajectory calculation) for the different airmass origins. For this evaluation a further subdivision in ascending airmasses from the boundary layer and descending airmasses from the free troposphere has been made, based on the vertical displacement of the back-trajectories. The differences in the trace gas levels for different airmass classes are quite small. In general, lower pollution levels are found for airmasses descending from the free troposphere. The highest pollution levels are observed for airmasses spending most of their time in the continental boundary layer over north-western Europe.

Beside photochemistry during the day, diurnal variations (Fig. 2) are mainly driven by local meteorology. Diurnal variations of trace gases at high-elevation mountainous sites are generally influenced by local catabatic and anabatic winds (Zaveri et al., 1995). After sunset, radiative cooling of the mountain slopes cools the adjacent air, resulting in downslope flows (catabatic winds). Therefore, high-elevation sites like Mt. Cimone often receive air from the free troposphere during the night. Shortly after sunrise, solar heating warms the air adjacent to the slopes, causing a reversal of the flow, giving rise to upslope (anabatic) winds, that can bring polluted air from the continental boundary layer to the site. At Mt. Cimone weak diurnal variations are observed for NO_x, NO_y, O_3 and CO (Fig. 2). As expected, pollutant levels are higher during the day (see Table 1), due to transport of boundary layer air to the site, but the ratio of NO_x/NO_y, which is approximately 0.3 (0.29 $\pm$ 0.16), indicates transport of photochemically processed airmasses to the site. An exception is the higher concentration of NO_y during the night.

This is partly due to a bias in the nighttime NO_y data due to the strong enhancements observed during the night of 9/10 June (see Fig. 1). Much stronger diurnal variations are observed for RO_x and HCHO. For these species the diurnal variation is much more dependent on local photochemistry rather than transport, producing high values during the day (Fig. 2 and Table 1).

Additional measurements of HNO_3 were performed by the Max Planck Institute for Nuclear Physics (Hanke et al., this issue). The calculated ratio between HNO_3 and NO_y is close to unity (mean $\pm 1\sigma$-standard deviation: 0.9 ± 2.8), with 40% of all ratios larger than one. A linear regression indicates a significant offset of the order of 0.5 ppbv ($HNO_3 = 0.36\ NO_y + 0.445$). This offset can be either due to an overestimation of HNO_3 or a corresponding underestimation of the measured NO_y. If we assume that HNO_3 is a rather constant fraction of NO_y, an underestimation of NO_y by a constant amount could be due to either inlet losses or an underestimation of the HNO_3 conversion efficiency of the converter. Since the NO_y converter itself acts as an inlet system, losses of HNO_3 are very low in our measurement set-up. In-field measurements of the conversion efficiency of the converter for HNO_3 were not made, but laboratory tests before and after the campaign demonstrated a good agreement between the HNO_3 conversion efficiency and those for NO_2 (97%) within 5% (Lange et al., 2002). Although we cannot exclude a systematic underestimation of the NO_y measurements by 0.5 ppbv, we nevertheless consider this as highly unlikely.

3.2. Comparison to observations at other remote mountainous sites

It is useful to compare the measurements at Mt. Cimone to spring or summer observations at other high elevation mountainous sites. Table 4 shows a comparison of mean O_3, CO, NO_x, NO_y, and HCHO trace gas levels, as well as average noontime RO_x concentrations observed at Mt. Cimone (Italy, 44.18° N, 10.7° E, 2165 m asl), Mauna Loa (Hawaii, 19.38° N, 155.36° W, 3400 m asl), Izana (Tenerife, 28.18° N, 16.3° W, 2370 m asl), Jungfraujoch (Swiss Alps, 46.33° N, 7.59° W, 3580 m asl), and Idaho Hill (Colorado, Rocky Mountains, 39.5° N, 105.37° W, 3070 m asl). The measurements at Mauna Loa

were obtained during the Mauna Loa Observatory Photochemistry Experiment (MLOPEX) II intensive measurement campaign between 15 July and 15 August 1992 (Atlas and Ridley, 1996), while the measurements at Izana were made during the Oxidizing Capacity of the Tropospheric Atmosphere (OCTA) intensive from 31 July until 22 August 1994

5   (Fischer et al., 1998). Both sites are in remote marine environments in the North Pacific and Atlantic Oceans, respectively. In general, their high elevations guarantee access to the free troposphere, at least during the night and the early morning hours. Contrary to these sites, Idaho Hill, the Jungfraujoch, and Mt. Cimone are located in North America and Europe, thus representing continental background conditions. Measurements

10 at Idaho Hill were obtained during the Tropospheric OH Photochemistry Experiment (TOPHE) in August/September 1993 (Mount and Williams, 1997). Intensive measurements at the Jungfraujoch were performed between 18 July and 23 August 1997 (Zellweger et al., 2000) and during the Free Tropospheric Experiment (FREETEX) between 19 March and 14 April 1998 (Carpenter et al., 2000). The data in Table 4 have been

15 subdivided into free tropospheric and boundary layer influenced airmasses by averaging nighttime and daytime measurements, respectively. In general the trace gas levels listed in Table 4 reflect the remoteness of the sites, with lowest pollution levels observed at Mauna Loa for downslope conditions at night. The concentration levels for NO_x, NO_y, CO, and O_3 at Mt. Cimone are very similar to the summer 1997 measurements at

20 the Jungfraujoch, indicating European continental background conditions. The HCHO levels at Mt. Cimone, Izana, and Idaho Hill are of the same order (0.9–1.4 ppbv), while observations at Mauna Loa indicate much smaller concentrations (0.15–0.3 ppbv). The noontime average RO_x levels vary within a factor of two for the four sites.

3.3.   Ozone production

25 The oxidation of CO and volatile organic compounds (VOC) in the presence of sufficient amounts of NO_x (= NO + NO_2) can be considered as a significant source of tropospheric ozone (Crutzen, 1973; Chameides and Walker, 1973; Liu et al., 1980). During daylight hours NO_2 is photolytically converted to NO leading to the formation of

O_3:

$$NO_2 + h\nu(\lambda < 424\,nm) \rightarrow NO + O \qquad (R1)$$

$$O + O_2 + M \rightarrow O_3 + M \qquad (R2)$$

Under most tropospheric conditions the dominant pathway by which NO is converted back to NO_2 is via the reaction with O_3:

$$NO + O_3 \rightarrow NO_2 + O_3 \qquad (R3)$$

The sequence of reactions (R1), (R2), and (R3) constitutes a cycle with no net O_3 production or destruction, but the photochemical oxidation of CO and VOC produces peroxy radicals (HO_2 and RO_2) that provide additional NO to NO_2 conversion routes:

$$NO + HO_2 \rightarrow NO_2 + OH \qquad (R4)$$

$$NO + RO_2 \rightarrow NO_2 + RO \qquad (R5)$$

In these reactions the conversion of NO to NO_2 does not consume O_3 so that the subsequent photolysis of NO_2 (reaction (R1) followed by reaction (R2)) represents a net source of O_3. The peroxy radicals needed in (R4) and (R5) are formed mainly in the photochemical oxidation of CO and CH_4:

$$CO + OH(+O_2) \rightarrow CO_2 + HO_2 \qquad (R6)$$

$$CH_4 + OH(+O_2) \rightarrow CH_3O_2 + H_2O \qquad (R7)$$

and in reactions of higher non-methane hydrocarbons with OH.

Under the assumption that ozone is formed mainly via the oxidation of methane the ozone production rate is given as (Liu et al., 1980):

$$P(O_3) = \left\{ k_{R4}[HO_2] + k_{R5}[CH_3O_2] \right\} [NO] \qquad (1)$$

Ozone production and trace gas correlations

H. Fischer et al.

Title Page

Abstract | Introduction

Conclusions | References

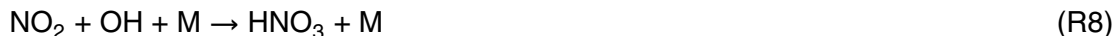Tables | Figures

◄◄ | ►►

◄ | ►

Back | Close

Full Screen / Esc

Print Version

Interactive Discussion

Note that through the reaction of NMHC with OH, RO_2 radicals other than CH_3O_2 are formed that can contribute to the ozone production.

The net ozone production is limited by radical termination reactions, e.g.:

$$NO_2 + OH + M \rightarrow HNO_3 + M \tag{R8}$$

dominating at high NO_x concentrations, and

$$HO_2 + HO_2 \rightarrow H_2O_2 + O_2 \tag{R9}$$

$$CH_3O_2 + HO_2 \rightarrow CH_3OOH + O_2 \tag{R10}$$

most significant at low NO_x concentrations.

Ozone is lost by photolysis, producing an oxygen atom in an electronically excited state

$$O_3 + h\nu\,(\lambda < 315\,\text{nm}) \rightarrow O_2 + O(^1D) \tag{R11}$$

that can either be quenched to the ground-state by collision with N_2 or O_2 or react with water vapour to form two hydroxyl radicals (OH):

$$O(^1D) + H_2O \rightarrow 2\,OH \tag{R12}$$

Additional losses of O_3 are due to its reaction with either OH or HO_2

$$OH + O_3 \rightarrow HO_2 + O_2 \tag{R13}$$

$$HO_2 + O_3 \rightarrow OH + 2\,O_2 \tag{R14}$$

If we assume that ozone losses due to dry deposition, heterogeneous reactions and up-take in cloud droplets, and reactions with alkenes are negligible, its loss term is

$$L(O_3) = \left(f\,j(O^1D) + k_{R13}[OH] + k_{R14}[HO_2] \right) [O_3] \tag{2}$$

where $j(O^1D)$ is the ozone photolysis rate and f is the fraction of $O(^1D)$ atoms reacting with H_2O to produce OH rather than being collisionally deactivated.

The difference between Eq. (1) and (2) describes the net ozone production:

$$NOP = P(O_3) - L(O_3) \tag{3}$$

Equation (3) can be evaluated using chemical box models (e.g. Liu et al., 1980) or estimated from in situ measurements of O_3, NO, $HO_2 + RO_2$, $j(O^1D)$, H_2O, and temperature (Penkett et al., 1997; Zanis et al., 2000b). Here we follow the approach described in detail by Zanis et al. (2000b). The OH concentration, which was not measured at the site, was estimated according to Zanis et al. (2000a):

$$\frac{[HO_2] + [CH_3O_2]}{[OH]} = \frac{k_{R6}[CO] + k_{R7}[CH_4] + k_{R1}[O_3]}{k_{R4}[NO] + k_{R14}[O_3] + 2\sqrt{k'j(O^1D)[O_3]}} \tag{4}$$

with $[CH_4] = 1800$ ppbv.

The coefficient k' is defined as

$$k' = (\beta^2 k_{R9} + \beta k_{R10} + k_{R(CH_3O_2+CH_3O_2)})/(\beta + 1)^2 \tag{5}$$

where $\beta = [HO_2]/[CH_3O_2]$.

As first shown by Penkett et al. (1997) scatter plots of $[HO_2] + [RO_2]$ versus $(j(O^1D))^{1/2}$ can be used to derive an experimental value for k' from the gradient of a fitted regression line on the data, while $\beta = 1$ was derived from in situ HO_2 and RO_2 measurements at Mt. Cimone using the Heidelberg ROXMAS instrument (Uecker et al., 2001). Note that Zanis et al. (2000b) derived a much higher value for β of 4–7 using a box model to simulate the HO_2/CH_3O_2 ratio at the Jungfraujoch. Sensitivity studies indicate that NOP would decrease by 11% for $\beta = 5$.

Figure 3 shows the mean daytime (06:00–20:00 GMT) net ozone production (NOP) rate ($\pm 1\sigma$-standard deviation), together with the average NO concentration. The NOP evaluated for the period between 14 June (DOY 166) and 28 June (DOY 180) varies

Ozone production and trace gas correlations

H. Fischer et al.

Print Version

Interactive Discussion

between approximately zero (23 June, DOY 175) and 0.2–0.3 ppbv/hr. The average daily NO concentration is approximately 40 pptv. This is comparable to the daily average net ozone production rates deduced for the Jungfraujoch during the FREETEX'98 campaign in March/April 1998, that varied from around 0.1 ppbv/hr for relatively clean
5   days to more than 1 ppbv/hr during the more polluted days at average daily NO mixing ratios of 27.3 and 260.5 pptv, respectively (Zanis et al., 2000b). Contrary to the positive NOP derived for these two mountainous sites in continental Europe, Cantrell et al. (1996) deduced a negative NOP (-0.15 ppbv/hr) for a mean NO concentration of 19 pptv at Mauna Loa during MLOPEX II in summer 1992, a remote site in the central
10   North Pacific.

3.4.   Trace gas relations

In the preceding section we used a present-time frame method based on observational quantities to estimate the on-site net ozone production at Mt. Cimone. To describe the net O_3 production during the transport of airmasses to the site, past-time frame
15   techniques can be applied (Kleinman, 2000). Such methods are generally based on relations among O_3 with CO, NO_y or NO_z (= NO_y - NO_x) (for a recent review see Trainer et al., 2000). A positive correlation between O_3 and CO can be expected if one assumes that CO is a proxy for the amount of reactive carbon (CO and hydrocarbons) used during O_3 production (Fishman et al., 1980; Fischer et al., 2002). A slope of ~ 0.3
20   has been observed in O_3-CO scatter plots at various rural and remote sites in moderately polluted boundary layer air (Parrish et al., 1993, 1998; Chin et al., 1994), while no significant correlation is found in the middle and upper troposphere (Fishman et al., 1980, 2002). Figure 4 shows O_3-CO scatter plots for the measurements at Mt. Cimone. Positive correlations between these species are observed during day and night with
25   slopes of the order of 0.25, similar to observations at other sites in North America (Chin et al., 1994), the Atlantic coast of Canada (Parrish et al., 1993) and the central Atlantic ocean (Fischer et al., 1998; Parrish et al., 1998) during summer.

Nevertheless, the correlation coefficients of the O_3-CO relations at Mt. Cimone are

rather small, most probably indicating significant contributions to the O_3 budget at the site associated with transport from the middle and upper free troposphere.

Trainer et al. (1993) found that a positive correlation exists between O_3 and the oxidation products of NO_x, i.e. $NO_z = NO_y - NO_x$. This is a consequence of the fact that the rate of ozone formation is indirectly related to the rate of NO_x oxidation to NO_z (Liu et al., 1987; Trainer et al., 1993). Thus the slope of O_3-NO_z scatter plots has been interpreted as an estimate of the amount of O_3 formed per ppbv of NO_x oxidized. However, this slope is further affected by the relative rates of chemical and physical (dry deposition and rainout) removal of O_3 and NO_z (in particular its major constituent HNO_3), and by the mixing of air parcels of different histories (Trainer et al., 2000). Therefore, the slope of an O_3-NO_z scatter plot in general provides only a lower limit of the gross ozone production efficiency. Figure 5 shows the correlation among these species obtained at Mt. Cimone. The slope is about 9 which is comparable to observations in the eastern United States that showed values of $\Delta O_3 / \Delta NO_z$ between 8 and 12 (e.g. Trainer et al., 1993; Poulida et al., 1994; Kleinmann et al, 1994). Lower values of 4–6 $\Delta O_3 / \Delta NO_z$ were observed in the city plume of Freiburg at Schauinsland (Volz-Thomas et al., 1993). The large scatter and the subdivision into two branches in Fig. 5 is most probably due to dry deposition and rainout of HNO_3, or mixing of airmasses with different histories, both of which tend to modify the slope of the regression and the correlation coefficient. The upper branch in Fig. 5 consists of data points with high O_3 values (> 75 ppbv). These data are mainly due to observations made during late afternoons of 2, 3, and 9 June. In particular the pollution event in the late afternoon (18:00–23:00 GMT) of 9 June, when the highest concentrations of NO_x, NO_y, O_3 and HCHO were observed, contributes to this particular branch of the O_3-NO_z correlation ($R^2 = 0.54$). The slope of the regression analysis for this branch is 9.4 indicating rather high ozone production in freshly polluted airmasses ($NO_x/NO_y > 0.3$). Note that this branch is not present in the O_3-CO scatter plot, since CO measurements are not available before 14 June. The lower branch in Fig. 5 is characterized by NO_z values in excess of 1.5 ppbv and O_3 values less than 75 ppbv ($R^2 = 0.45$). These airmasses are characterized by signifi-

© EGU 2002

cantly smaller NO_x/NO_y ratios (< 0.2) indicating more processed air (during the nights of 1–2, 16–17 June and during the day of 18 June).

Much higher correlation coefficients are observed for a number of scatter plots involving HCHO, an intermediate in the oxidation of methane and higher hydrocarbons. A particularly significant correlation was observed for HCHO and CO (overall $R^2 = 0.54$) (Fig. 6), while weaker correlations were observed for HCHO and NO_y (overall $R^2 = 0.4$) (Fig. 7) and HCHO and O_3 (overall $R^2 = 0.37$) (Fig. 8). The HCHO-NO_y scatter plot is again composed of two branches, corresponding to the airmass classification discussed already for the O_3-NO_z relation. Here the freshly polluted airmass has higher HCHO levels (> 2 ppbv), than the more processed, aged airmass (HCHO < 2 ppbv). Again this separation cannot be identified in the HCHO-CO scatter plot due to the missing CO measurements before 14 June. In the HCHO-O_3 scatter plot the plume associated with the freshly polluted airmass is clearly visible at $O_3 > 75$ ppbv.

If one restricts the analysis to those days that were not affected by clouds (clear sky days: DOY 155, 157, 165, 171, 173, 174, 175) the HCHO vs. CO and HCHO vs. NO_y correlations are even stronger with $R^2 = 0.73$ and 0.82, respectively. On the other hand, the effect of the data filtering on the correlation coefficients for HCHO vs. O_3, O_3 vs. NO_z and O_3 vs. CO is not significant.

A correlation between CO and HCHO is usually interpreted as an indication of nearby anthropogenic emission sources (Neitzert and Seiler, 1981; Cardenas et al., 1999) or the influence of biomass burning (Mauzerall et al., 1998). Nevertheless, a positive correlation among these species has recently been observed in the remote marine boundary layer over the Indian Ocean, far away from anthropogenic or biomass burning sources (Wagner et al., 2001). To estimate the contribution from direct emissions, the HCHO/CO area emission ratio for eastern North America $5.6 \cdot 10^{-3}$ (Li et al., 1994) is used. The slope of the regression analysis for Fig. 6 gives a ratio almost an order of magnitude higher ($3 \cdot 10^{-2}$), confirming that direct emissions most probably contribute little to the observed correlation. It is likely that secondary HCHO formation from volatile organic compounds is at least partially responsible for the observed correlation. In this

Title Page

Abstract | Introduction

Conclusions | References

Tables | Figures

◄◄ | ►►

◄ | ►

Back | Close

Full Screen / Esc

Print Version

Interactive Discussion

case CO would serve as a proxy for VOCs associated with combustion processes, which is further supported by the observed correlation of NO_y vs. HCHO (Fig. 7) and NO_y vs. CO (not shown).

4. Summary and conclusions

5 Continuous trace gas measurements of O_3, CO, NO, NO_2, NO_y, HCHO and RO_x, together with the photolysis rate of O_3 ($j(O^1D)$) and analysis of canister samples for VOCs were made during the MINATROC intensive summer campaign at the Mt. Cimone station (Italy, 44° 11′ N–10° 42′ E, 2165 m asl) between 1 and 30 June 2000. In general, mean trace gas mixing ratios are relatively low (CO = (121 ± 20) ppbv, NO_x = (0.284 ±

10 0.220) ppbv, NO_y = (1.15 ± 0.8) ppbv, O_3= (58 ± 9 ppbv)) (Table 1), which points to a low level of local pollution. This is further supported by the analysis of VOCs, with average levels typical for background continental air (e.g. C_2H_6 = (905 ± 200) pptv, C_3H_8 = (268 ± 110) pptv, C_2H_2 = (201 ± 102) pptv, C_5H_8 = (111 ± 124) pptv, benzene = (65 ± 33) pptv). The trace gas levels at Mt. Cimone are comparable to measurements at

15 two other mountain sites, the Jungfraujoch in the Swiss Alps (Zanis et al., 2000b) and Idaho Hill, Colorado (Cantrell et al., 1997; Harder et al., 1997; Williams et al., 1997), while they are higher than observations at the remote N-Pacific location Mauna Loa (Atlas and Ridley, 1996; Cantrell et al., 1996; Zhou et al., 1997).

Average mid-day peroxy radical concentrations at Mt. Cimone are of the order of

20 30 pptv. At mean NO concentrations of the order of 40 pptv this gives rise to significant in situ net O_3 production at the site (0.1–0.3 ppbv/hr).

Significant photochemical O_3 production is further supported by correlations between O_3, CO, or NO_z. The slopes of these correlations (~ 0.3 for O_3/CO; ~ 9 for O_3/NO_z) are comparable to reported observations from North America, Europe, or the

25 central Atlantic (Trainer et al., 1993; Parrish et al., 1993, 1998; Poulida et al., 1994; Kleinmann et al., 1994; Chin et al., 1994; Fischer et al., 1998). The large slope of the observed HCHO/CO correlation indicates that HCHO production at the site has a

Ozone production and trace gas correlations

H. Fischer et al.

Title Page

Abstract	Introduction
Conclusions	References
Tables	Figures

| ◀◀ | ▶▶ |
| ◀ | ▶ |

| Back | Close |

Full Screen / Esc

Print Version

Interactive Discussion

strong contribution from the oxidation of longer lived VOCs that are emitted along with CO. The fact that HCHO is also significantly correlated with NO_y (NO_y itself is strongly correlated with CO) indicates that the HCHO precursors are mainly associated with anthropogenic combustion processes.

References

Atlas, E. L. and Ridley, B. A.: The Mauna Loa Observatory Photochemistry Experiment: Introduction, J. Geophys. Res., 101, 14 531–14 541, 1996.

Balkanski, Y., Bauer, S. E., van Dingenen, R., Bonasoni, P., Schulz, M., Fiscer, H., Gobbi, G. P., Hanke, M., Hauglustaine, D., Putaud, J. P., and Stohl, A.: Overall p resentation of the campaign of Mt. Cimone, Italy; principle characteristics of the gaseous and aerosol composition from European pollution, Mediterranean influences, and during African dust events, Atmos. Chem. Phys. Discuss., this issue, 2002.

Bonasoni, P., Stohl, A., Cristofanelli, P., Calzolri, F., Colombo, T., and Evangelisti, F.: Background ozone variations at Mt. Cimone station, Atmos. Environm., 34, 5183–5189, 2000.

Bonasoni, P., Cristofanelli, P., van Dingenen, R., Calzolari, F., Bonafe, U., Colombo, T., Evangelista, F., Tositti, L., and Balkanski, Y.: Aerosol and ozone correlation during the transport episodes of the summer-autumn 2000 period, Atmos. Chem. Phys. Discuss., this issue, 2002.

Cantrell, C. A., Shetter, R. E., Gilpin, T. M., and Calvert, J. G.: Peroxy radical measured during the Mauna Loa Observatory Photochemistry Experiment 2: The data and first analysis, J. Geophys. Res., 101, 14 643–14 652, 1996.

Cantrell, C. A., Shetter, R. E., Calvert, J. G., Eisele, F. L., Williams, E., Baumann, K., Brune, W. H., Stevens, P. S., and Mather, J. H.: Peroxy radicals from photostationary state deviations and steady state calculations during the Tropospheric OH Photochemistry Experiment at Idaho Hill, Colorado, 1993, J. Geophys. Res., 102, 6369–6378, 1997.

Ozone production and trace gas correlations

H. Fischer et al.

© EGU 2002

Cardenas, L. M., Mills, G., and Penkett, S. A.: Tropospheric measurements of formaldehyde, Proceedings of EUROTRAC Symposium '98, 356–360, 1999.

Carpenter, L. J., Green, T. J., Mills, G. P., Bauguitte, S., Penkett, S. A., Zanis, P., Schuepbach, E., Schmidbauer, N., Monks, P. S., and Zellweger, C.: Oxidized nitrogen and ozone production efficiencies in the springtime free troposphere over the Alps, J. Geophys. Res., 105, 15 547–14 559, 2000.

Chameides, W. and Walker, J. C. G.: A photochemical theory of tropospheric ozone, J. Geophys. Res., 78, 8751–8760, 1973.

Chin, M., Jacob, D. J., Munger, J. W., Parrish, D. D., and Doddridge, B. G.: Relationship of ozone and carbon monoxide over North America, J. Geophys. Res., 99, 14 565–14 573, 1994.

Crutzen, P. J.: A discussion of the chemistry of some minor constituents in the stratosphere and troposphere, Pure Appl. Geophys., 106, 1385–1399, 1973.

Crutzen, P. J.: Ozone in the troposphere, in: Composition, Chemistry, and Climate of the Atmosphere, (Ed) Singh, H. B., Van Norstrand Reinhold, New York, pp. 349–393, 1995.

Fischer, H., Nikitas, C., Parchatka, U., Zenker, T., Harris, G. W., Matuska, P., Schmitt, R., Mihelcic, D., Muesgen, P., Paetz, H.-W., Schulz, M., and Volz-Thomas, A.: Trace gas measurements during the Oxidizing Capacity of the Tropospheric Atmosphere campaign 1993 at Izana, J. Geophys. Res., 103, 13 505–13 518, 1998.

Fischer, H., Brunner, D., Harris, G. W., Hoor, P., Lelieveld, J., McKenna, D. S., Rudolph, J., Scheeren, H. A., Siegmund, P., Wernli, H., Williams, J., and Wong, S.: Synoptic tracer gradients in the upper troposphere over central Canada during the STREAM 1998 summer campaign, J. Geophys. Res., 107(8),10.1029/2000JD000312, 2002.

Fishman, J., Seiler, W., and Haagenson, P.: Simultaneous presence of O_3 and CO bands in the troposphere, Tellus, 32, 456–463, 1980.

Harder, J. W., Fried, A., Sewell, S., and Henry, B.: Comparison of tunable diode laser and long-path ultraviolet/visible spectroscopic measurements of ambient formaldehyde concentrations during the 1993 OH Photochemistry Experiment, J. Geophys. Res., 102, 6267–6282, 1997.

Hanke, M., Uecker, J., Reiner, T., and Arnold, F.: Atmospheric peroxy radicals: ROXMAS, a new mass-spectrometric methodology for speciated measurements of HO_2 and ΣRO_2 and first results, Int. J. Mass Spectr., 213, 91–99, 2002.

Hanke, M., Umann, B., Uecker, J., Arnold, F., and Bunz, H.: Atmospheric measurements of gas-phase HNO_3 and SO_2 with chemical ionisation mass spectrometry during the first MI-

Ozone production and trace gas correlations

H. Fischer et al.

Title Page

Abstract	Introduction
Conclusions	References
Tables	Figures

◄◄   ►►

◄   ►

Back   Close

Full Screen / Esc

Print Version

Interactive Discussion

NATROC filed campaign at Mt. Cimone, 2000, Atmos. Chem. Phys. Discuss., this issue, 2002.

Hastie, D. R., Weissenmayer, M., Burrows, J. P., and Harris, G. W.: Calibrated chemical amplifier for atmospheric RO$_x$ measurements, Anal. Chem., 63, 2048–2057, 1991.

5 Holton, J. R., Haynes, P. H., McIntyre, M. E., Douglass, A. R., Rood, R. B., and Pfister, L.: Stratosphere-troposphere exchange, Rev. of Geophys., 33, 403–439, 1995.

Kleinman, L., Lee, Y.-N., Sprinston, S. R., Nunnermacker, L., Zhou, X., Brown, R., Hallock, K., Klotz, P., Leahy, D., Lee, J. H., and Newman, L.: Ozone formation at a rural site in the southern United States, J. Geophys. Res., 99, 3469–3482, 1994.

10 Kleinman, L. I.: Ozone production insights from field experiments – part II: Observation-based analysis for ozone production, Atmos. Environm., 34, 2023–2033, 2000.

Kormann, R., Fischer, H., Gurk, C., Helleis, F., Klüpfel, Th., Königstedt, R., Parchatka, U., and Wagner, V.: Application of TRISTAR, a three-laser tunable diode laser absorption spectrometer during MINATROC, Spectrochimica Acta, A58, 2489–2498, 2002.

15 Lange, L., Fischer, H., Parchatka, U., Gurk, C., Zenker, T., and Harris, G. W.: Characterization of an externally mounted catalytic converter for aircraft measurements, Rev. Scient. Instr., 73, 3051–3057, 2002.

Li, S.-M., Anlauf, K. G., Wiebe, A., and Bottenheim, J. W.: Estimating primary and secondary production of HCHO in eastern North America based on gas phase measurements and 20 principal component analysis, Geophys. Res. Lett., 21, 669–672, 1994.

Liu, S. C., Kley, D., McFarland, M., Mahlmann, J. D., and Levy, II, H.: On the origin of tropospheric ozone, J. Geophys. Res., 85, 7546–7552, 1980.

Liu, S. C., Trainer, M., Fehsenfeld, F. C., Parrish, D. D., Williams, E. J., Fahey, D. W., Hübler, G., and Murphy, P. C.: Ozone production in the rural troposphere and the implications for 25 regional and global ozone distributions, J. Geophys. Res., 92, 4191–4207, 1987.

Mauzerall, D. L., Logan, J. A., Jacob, D. J., Anderson, B. E., Blake, D. R., Bradshaw, J. D., Heikes, B., Sachse, G. W., Singh, H., and Talbot, B.: Photochemistry in biomass burning plumes and implications for tropospheric ozone over the tropical South Atlantic, J. Geophys. Res., 103, 8401–8423, 1998.

30 Mihele, C. M. and Hastie, D. R.: The sensitivity of the radical amplifier to ambient water vapour, Geophys. Res. Lett., 25, 1911–1913, 1998.

Mount, G. H. and Williams, E. J.: An overview of the Tropospheric OH Photochemistry Experiment, Fritz Peak/Idaho Hill, Colorado, fall 1993, J. Geophys. Res., 102, 6171–6186, 1997.

Mühle, J., Zahn, A., Brenninkmeijer, C. A. M., Gros, V., and Crutzen, P. J.: Air mass classification during the INDOEX R/V Ronald Brown cruise using measurements of non-methane hydrocarbons, CH_4, CO_2, CO, ^{14}CO and $\partial^{18}O(CO)$, J. Geophys. Res., 107 (D19), 10.1029/2001JD000730, 2002.

5 Neitzert, V. and Seiler, W.: Measurement of formaldehyde in clean air, Geophys. Res. Lett., 8, 79–82, 1981.

Parrish, D. D., Holloway, J. S., Trainer, M., Murphy, P. C., Forbes, G. L., and Fehsenfeld, F. C.: Export of North American ozone pollution to the North Atlantic Ozean, Science, 259, 1436–1439, 1993.

10 Parrish, D. D., Trainer, M., Holloway, J. S., Yee, J. E., Warshawsky, M., Fehsenfeld, F. C., Forbes, G. L., and Moody, J. L.: Relationships between ozone and carbon monoxide at surface sites in the North Atlantic region, J. Geophys. Res., 103, 13 357–13 376, 1998.

Penkett, S. A., Monks, P. S., Carpenter, L. J., Clemitshaw, K. C., Ayers, G. P., Gillet, R. W., Galbally, I. E., and Meyer, C. P.: Relationships between ozone photolysis rates and peroxy
15 radical concentrations in clean marine air over the southern ozean, J. Geophys. Res., 102, 12 805–12 817, 1997.

Perner, D., Arnold, T., Crowley, J., Klüpfel, T., Martinez, M., and Seuwen, R.: The measurement of active chlorine in the atmosphere by chemical amplification, J. Atmos. Chem., 34, 9–20, 1999.

20 Poulida, O., Civerolo, K. L., and Dickerson, R. E.: Observations and tropospheric photochemistry in central North Carolina, J. Geophys. Res., 99, 10 553–10 563, 1994.

Ridley, B. A. and Robinson, E.: The Mauna Loa photochemistry experiment, J. Geophys. Res., 97, 10 285–10 290, 1992.

Schultz, M., Heitlinger, M., Mihelcic, D., and Volz-Thomas, A.: Calibration source for peroxy
25 radicals with built-in actinometry using H_2O and O_2 photolysis at 185 nm, J. Geophys. Res., 100, 18 811–18 816, 1995.

Stohl, A., Wotawa, G., Seibert, P., and Kromp-Kolb, H.: Interpolation errors in wind fields as a function of spatial and temporal resolution and their impact on different types of kinematic trajectories, J. Appl. Meteorology, 34, 2149–2165, 1995.

30 Trainer, M., Parrish, D. D., Buhr, M. P., Norton, R. B., Fehsenfeld, F. C., Anlauf, K. G., Bottenheim, J. W., Tang, Y. Z., Wiebe, H. A., Roberts, J. M., Tanner, R. L., Newman, L., Bowersox, V. C., Meagher, J. F., Olszyna, K. J., Rodgers, M. O., Wang, T., Berresheim, H., Demerjian, K. L., and Roychowdhury, U. K.: Correlation of ozone with NO_y in photochemically aged air,

Ozone production and trace gas correlations

H. Fischer et al.

[Title Page](#)	
[Abstract](#)	[Introduction](#)
[Conclusions](#)	[References](#)
[Tables](#)	[Figures](#)

◄◄	►►
◄	►
Back	Close

Full Screen / Esc

[Print Version](#)

[Interactive Discussion](#)

J. Geophys. Res., 98, 2917–2925, 1993.

Trainer, M., Parrish, D. D., Goldon, P. D., Roberts, J., and Fehsenfeld, F. C.: Review of the observation-based analysis of the regional factors influencing ozone concentrations, Atmos. Environ., 34, 2045–2061, 2000.

5 Uecker, J., Hanke, M., and Arnold, F.: First speciated atmospheric measurements of HO_2 and organic peroxy radicals (ΣRO_2) by chemical conversion/ion molecule reaction mass spectrometry (ROXMAS) before, during and after the major mineral dust intrusion on Monte Cimone during the first MINATROC field campaign in June–July 2000, Proceedings of the 8th European Symposium on the Physico-Chemical Behaviour of Atmospheric Pollutants, 17–20
10 September 2001, Torino (IT), (Eds) Hjorth, J., Raes, F., and Angeletti, G., 2001.

van Dingenen, R., Putaud, J. P., Roselli, D., Dell'Acqua, A., Perrone, M. P., Bonasoni, P., and Facchini, M. C.: Comprehensive characterisation of aerosol physical and chemical properties of the aerosol at Mt. Cimone, Atmos. Chem. Phys. Discuss., this issue, 2002.

Volz-Thomas, A., et al.: Photo-oxidants and precursors at Schauinsland, Black Forest, Proc.
15 EUROTRAC Symposium '92, (Eds) Borrell, P. M., et al., pp. 98–103, SPB Academic Publishing, The Hague, The Netherlands, 1993.

Wagner V., Schiller, C., and Fischer, H.: Formaldehyde measurements in the marine boundary layer of the Indian Ocean during the 1999 INDOEX cruise of the RV Ronald H. Brown, J. Geophys. Res., 106, 28 529–28 538, 2001.

20 Wagner, V., von Glasow, R., Fischer, H., and Crutzen, P. J.: Are CH_2O measurements in the marine boundary layer suitable for testing the current understanding of the CH_4 photooxidation? – A model study, J. Geophys. Res., 107(3), 10-1029/2001JD000722, 2002.

Wienhold, F. G., Fischer, H., Hoor, P., Wagner, V., Königstedt, R., Harris, G. W., Anders, J., Grisar, R., Knothe, M., Riedel, W. J., Lübken, F.-J., and Schilling, T.: TRISTAR – a tracer in
25 situ TDLAS for atmospheric research, Appl. Phys. B, 67, 411–417, 1998.

Williams, E. J., Roberts, J. M., Baumann, K., Bertman, S. B., Buhr, S., Norton, R. B., and Fehsenfeld, F. C.: Variations in NO_y composition at Idaho Hill, Colorado, J. Geophys. Res., 102, 6297–6314, 1997.

Zanis, P., Monks, P. S., Schuepbach, E., and Penkett, S. A.: The role of in situ photochemistry
30 in the control of ozone during spring at the Jungfraujoch (3,580 m asl) – Comparison of model results with measurements, J. Atmos. Chem., 37, 1–27, 2000a.

Zanis, P., Monks, P. S., Schuepbach, E., Carpenter, L. J., Green, T. J., Mills, G. P., Bauguitte, S., and Penkett, S. A.: In situ ozone production under free tropospheric conditions during

Ozone production and trace gas correlations

H. Fischer et al.

[Title Page](#)	
[Abstract](#)	[Introduction](#)
[Conclusions](#)	[References](#)
[Tables](#)	[Figures](#)
[◄◄](#)	[►►](#)
[◄](#)	[►](#)
[Back](#)	[Close](#)
[Full Screen / Esc](#)	
[Print Version](#)	
[Interactive Discussion](#)	

FREETEX '98 in the Swiss alps, J. Geophys. Res., 105, 24 223–24 234, 2000b.

Zaveri, R. A., Saylor, R. D., Peters, L. K., McNider, R., and Song, A.: A model investigation of summertime diurnal ozone behaviour in rural mountainous locations, Atmos. Environm., 29, 1043–1065, 1995.

5 Zellweger, C., Ammann, M., Buchmann, B., Hofer, P., Lugauer, M., Rüttimann, R., Streit, N., Weingartner, E., and Bltensperger, U.: Summertime NO_y speciation at the Jungfraujoch, 3580 m above sea level, Switzerland, J. Geophys. Res., 105, 6655–6667, 2000.

Zhou, X., Lee, Y.-N., Newman, L., Chen, X., and Mopper, K.: Tropospheric formaldehyde concentration at the Mauna Loa Observatory Photochemistry Experiment 2, J. Geophys.
10 Res., 101, 14 7110–14 719, 1997.

Ozone production and trace gas correlations

H. Fischer et al.

Title Page

Abstract	Introduction
Conclusions	References
Tables	Figures

|◄   ►|

◄   ►

Back   Close

Full Screen / Esc

Print Version

Interactive Discussion

Table 1. Statistics of trace gas measurements (30 min resolution) during upslope (06:00–20:00 GMT) and downslope (20:00–06:00 GMT) conditions

	O_3/ppbv	CO/ppbv	NO_x/ppbv	NO_y/ppbv	CH_2O/ppbv	RO_x/pptv
All data:						
Mean	58	121	0.284	1.151	1.356	11
Median	57	121	0.241	0.983	1.296	7
1σ-STD	9	20	0.220	0.807	0.721	11
Central 50%	52 – 63	120 – 129	0.155–0.341	0.623–1.442	0.869–1.682	1 – 20
Range	31 – 103	84 – 330	0–2.119	0.019–5.885	0.106–4.992	−4 – 54
Number	1163	644	1143	1004	1134	1088
06:00–20:00 GMT:						
Mean	57	124	0.306	1.138	1.512	18
Median	56	119	0.267	0.897	1.418	17
1σ-STD	9	24	0.204	0.999	0.692	11
Central 50%	51 – 61	108 – 124	0.193–0.365	0.447–1.400	1.039–1.840	9 – 25
Range	31 – 103	84 – 330	0–2.119	0.019–5.855	0.262–4.992	−2 – 54
Number	705	370	664	415	650	654
20:00–06:00 GMT:						
Mean	60	117	0.253	1.159	1.145	1
Median	60	118	0.197	1.027	1.107	1
1σ-STD	9	13	0.237	0.639	0.707	2
Central 50%	54 – 65	108 – 125	0.112–0.295	0.713–1.480	0.580–1.482	0 – 2
Range	40 – 96	85 – 151	0–1.879	0.113–5.065	0.106–4.442	−4 – 12
Number	458	274	479	589	484	434

Table 2. Mean trace gas levels and standard deviations in pptv for NMHC measurements based on 26 canister samples collected between 6 June and 4 July 2000

NMHCs	Range	Mean	1σ-STD
Ethane	575–1446	905	200
Ethene	66–512	261	120
Propane	87–610	268	110
Propene	25–183	75	39
Isobutane	18–255	96	50
Butane	13–387	108	68
Acetylene	67–576	201	102
trans-2-Butene	1–11	5	2
1-Butene	6–37	15	8
cis-2-Butene	1–15	7	3
2-Methylbutane	12–446	110	86
Pentane	4–138	35	26
Cyclohexan	0–29	6	7
2-Methylpentane	2–92	26	19
3-Methylpentane	1–47	14	10
Hexane	3–32	13	7
Isoprene	0–500	111	124
Benzene	22–188	65	33

Ozone production and trace gas correlations

H. Fischer et al.

Table 3. Mean trace gas levels for different airmass classifications based on 3-D-back trajectories. One-sigma standard deviations are given in parenthesis. For the evaluation descending (FT) and ascending (BL) trajectories have been listed separately

	Altitude	%	CO / ppbv	HCHO / ppbv	NO_x / ppbv	NO_y / ppbv	O_3 / ppbv
Arctic	BL	NA	NA	NA	NA	NA	NA
	FT	1	112(5)	0.230(0.047)	0.111(0.039)	0.250(0.063)	63(5)
NW-Europe	BL	9	131(8)	1.588(0.492)	0.387(0.205)	2.059(0.997)	60(8)
	FT	5	129(5)	1.484(0.368)	0.265(0.081)	1.693(0.662)	60(6)
W-Europe	BL	15	120(8)	1.322(0.533)	0.267(0.117)	1.116(0.766)	56(10)
	FT	9	118(6)	1.527(0.676)	0.270(0.117)	0.999(0.651)	64(8)
E-Europe	BL	11	119(15)	1.283(0.580)	0.271(0.184)	1.216(0.633)	60(7)
	FT	7	113(17)	1.212(0.874)	0.184(0.119)	0.758(0.481)	53(7)
Mediterranian	BL	26	128(46)	1.314(0.754)	0.321(0.502)	0.945(0.747)	57(8)
	FT	6	106(10)	0.956(0.494)	0.337(0.162)	0.531(0.277)	55(6)
Africa	BL	6	NA	1.639(1.049)	0.351(0.666)	1.158(0.666)	57(10)
	FT	NA	NA	NA	NA	NA	NA

Title Page

Abstract | Introduction

Conclusions | References

Tables | Figures

◄◄ | ►►

◄ | ►

Back | Close

Full Screen / Esc

Print Version

Interactive Discussion

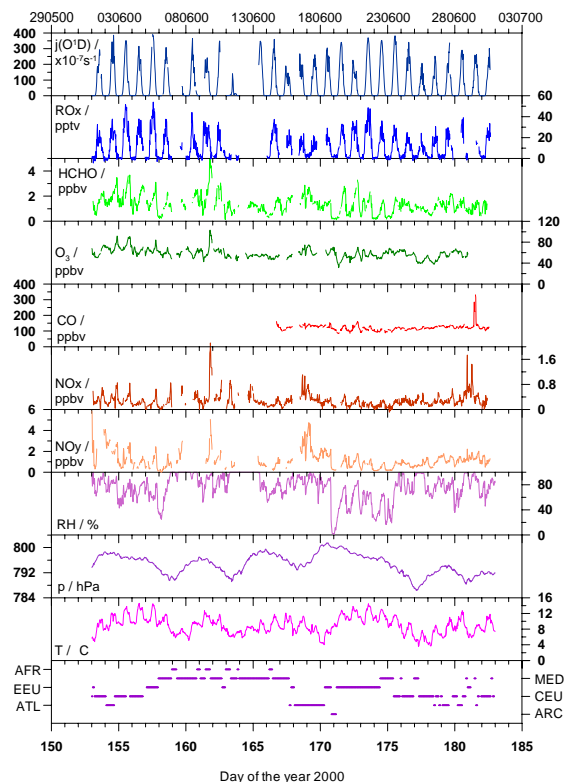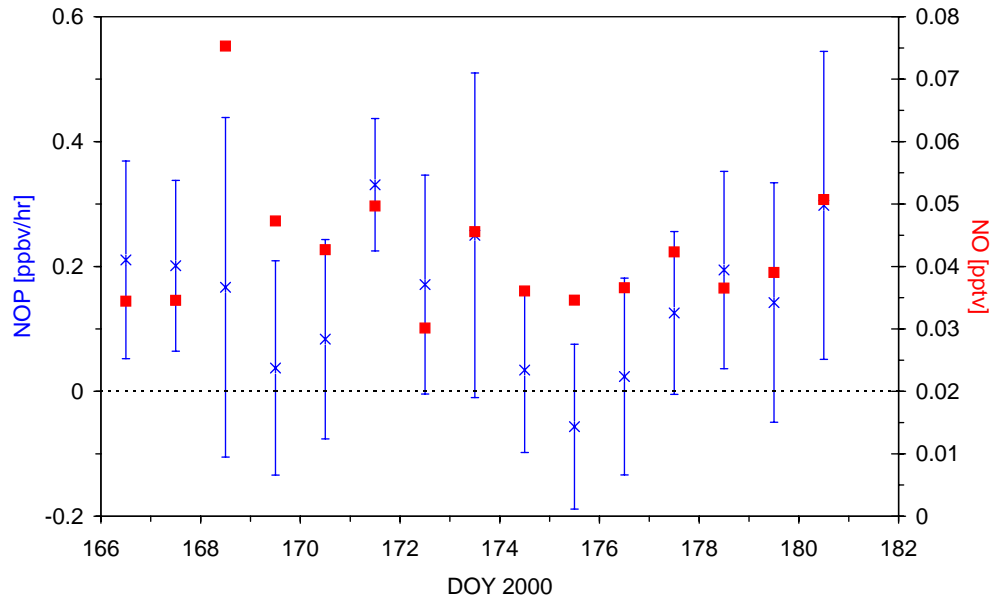**Ozone production
and trace gas
correlations**

H. Fischer et al.

**Table 4.** Comparison of trace levels (upslope/downslope conditions) observed at Mt. Cimone with summer time observations at four other mountainous sites in Europe and the US. The cited RO_x levels are average values for noontime

	Mt. Cimone	Mauna Loa[1]	Izana[2]	Jungfraujoch[3]	Jungfraujoch[4]	Idaho Hill[5]
Lat./Long.	44.18° N/10.7° E	19.38° N/155.36° W	28.18° N/16.3° W	46.33° N/7.59° W	46.33° N/7.59° W	39.5° N/105.37° W
Altitude [m]	2165	3400	2370	3580	3580	3070
Season	Jun 2000	Jul/Aug 1992	Jul/Aug 1994	Summer 1997	Mar/Apr 1998	Aug/Sep 1993
O_3 [ppbv]	56 / 60	33.8 / 35.6	38 / 40	49 / 44	57.8 / 59.8	51
CO [ppbv]	119 / 118	64 / 66	92 / 89	106 / 92	193 / 184	92
NO_x [pptv]	267 / 197	50 / 26	76 / 47	188 / 77	297 / 59	2221 / 393
NO_y [pptv]	897 / 1027	223 / 188	519 / 392	958 / 231	956 / 625	4315 / 1340
HCHO [ppbv]	1.4 / 1.1	0.3 / 0.15	1.4 / 1.1	n.a.	n.a.	1.4 / 0.9
RO_x [pptv]	30.5	25.4	65	n.a.	17.5	32

[1] Atlas and Ridley, (1996); Cantrell et al. (1996); Zhou et al. (1996)
[2] Fischer et al. (1998)
[3] Zellweger et al. (2000)
[4] Carpenter et al. (2000)
[5] Cantrell et al. (1997); Harder et al. (1997); Williams et al. (1997)

Ozone production and trace gas correlations

H. Fischer et al.

Fig. 1. Time series (30 min resolution) of trace gas mixing ratios, ozone photolysis rate, and meteorological parameters obtained during the MINATROC intensive campaign at Mt. Cimone, Italy. The lower panel indicates the airmass origin (Arctic (ARC), North-Western Europe (NWEU), Western Europe (WEU), Eastern Europe (EEU), Mediterranean Basin (MED), Saharan-African (AFR)) deduced from 144-hour backward-trajectories.
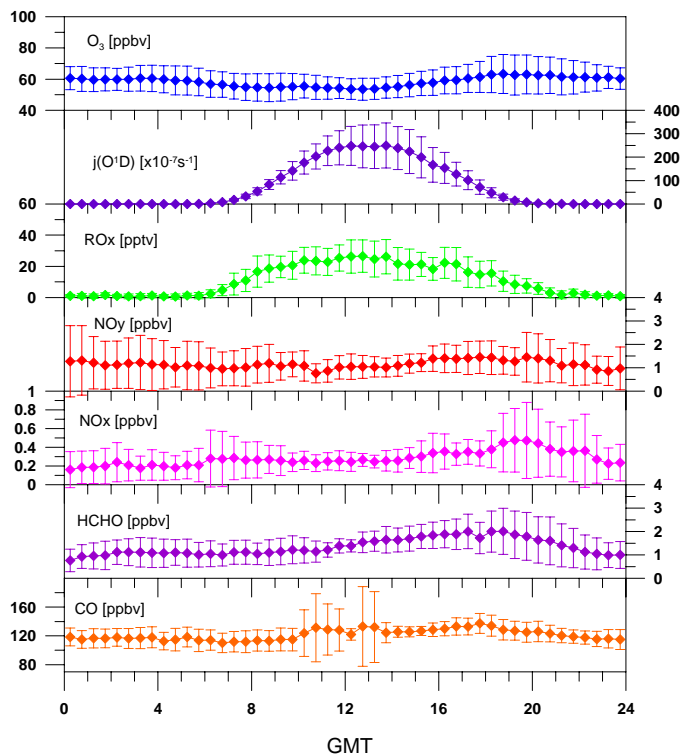
Fig. 2. Diurnal variation (mean ±1σ-standard deviation) of trace gas measurements at Mt. Cimone.

© EGU 2002

Fig. 3. Calculated daily mean (06:00–20:00 GMT) net ozone production (NOP) for the period between 14 June (DOY 166) and 28 June (DOY 180) (blue stars). The error bars indicate the 1σ-standard deviation. Red squares give the mean daytime NO concentration. Note that NO spikes due to local pollution have been omitted for this analysis.
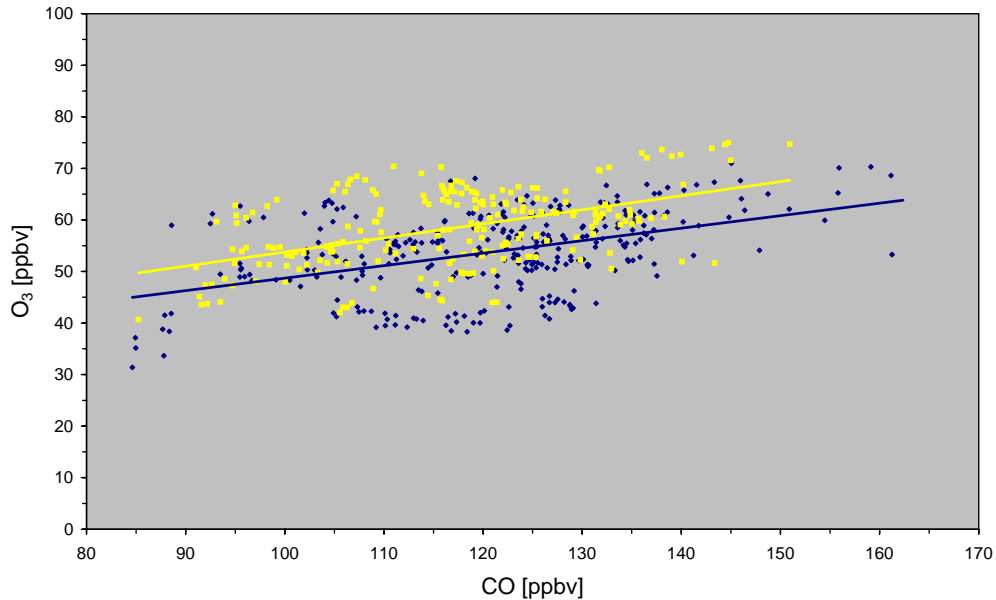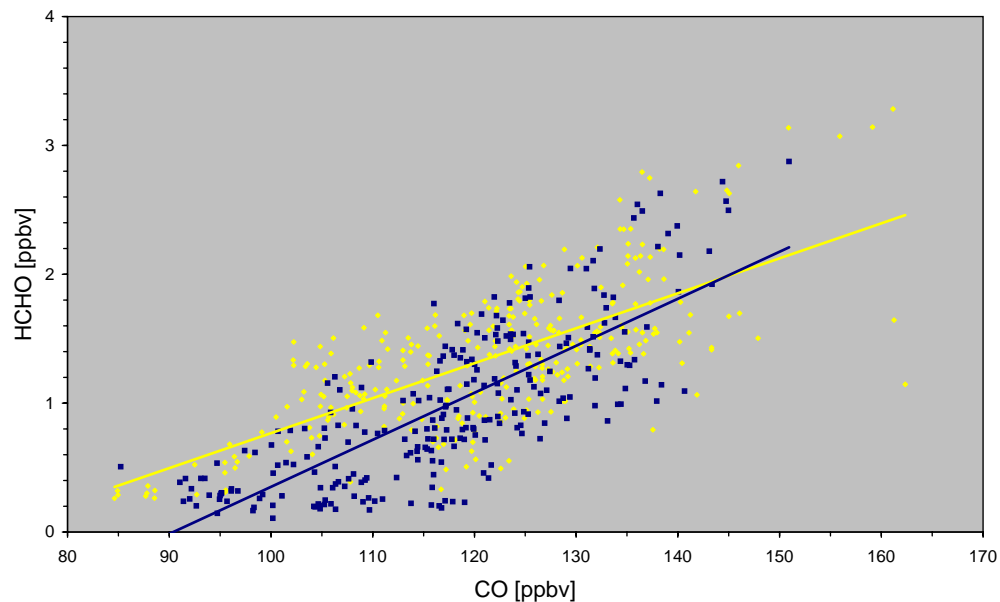
Fig. 4. Scatter plot of O_3 versus CO. Daytime data (06:00–20:00 GMT) are printed as yellow squares, while nighttime (20:00–06:00 GMT) observations are printed as dark blue diamonds. The individual regression lines for day and night are shown as yellow ($O_3 = 0.24$ CO $+ 24$; $R^2 = 0.19$) and blue ($O_3 = 0.27$ CO $+ 26$; $R^2 = 0.23$) lines, respectively. A linear regression analysis for the combined data yields: $O_3 = 0.22$ CO $+ 29$; $R^2 = 0.15$.

Title Page

Abstract | Introduction

Conclusions | References

Tables | Figures

|◄ | ►|

◄ | ►

Back | Close

Full Screen / Esc

Print Version

Interactive Discussion
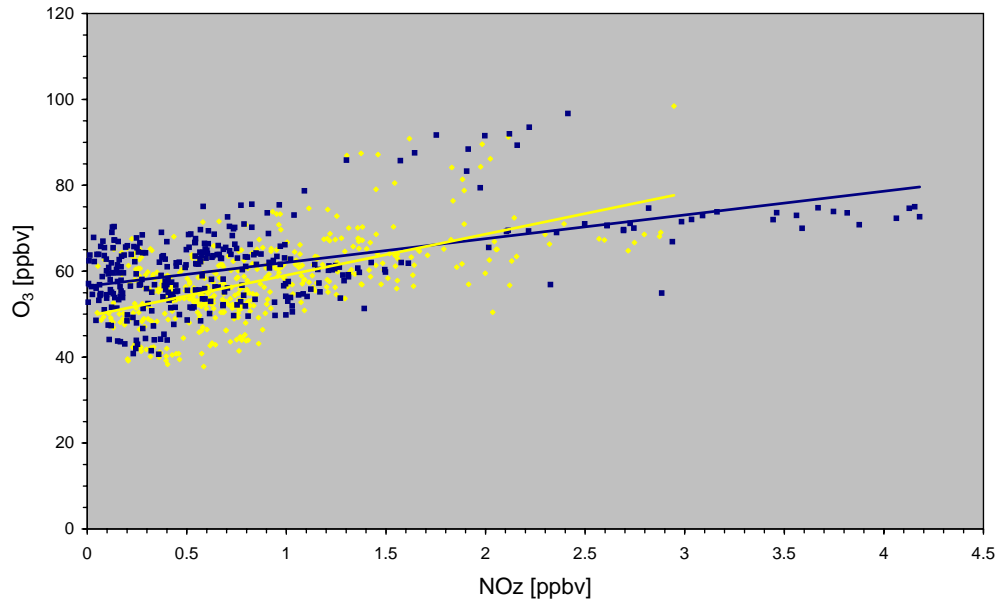
Fig. 5. Scatter plot of O_3 versus NO_z, defined as the difference between NO_y and NO_x. Daytime data (06:00–20:00 GMT) are printed as yellow squares, while nighttime (20:00–06:00 GMT) observations are printed as dark blue diamonds. The individual regression lines for day and night are shown as yellow ($O_3 = 9.6\ NO_z + 49$; $R^2 = 0.33$) and blue ($O_3 = 8\ NO_z + 54$; $R^2 = 0.22$) lines, respectively. A linear regression analysis for the combined data yields: $O_3 = 7\ NO_z + 53$; $R^2 = 0.27$.
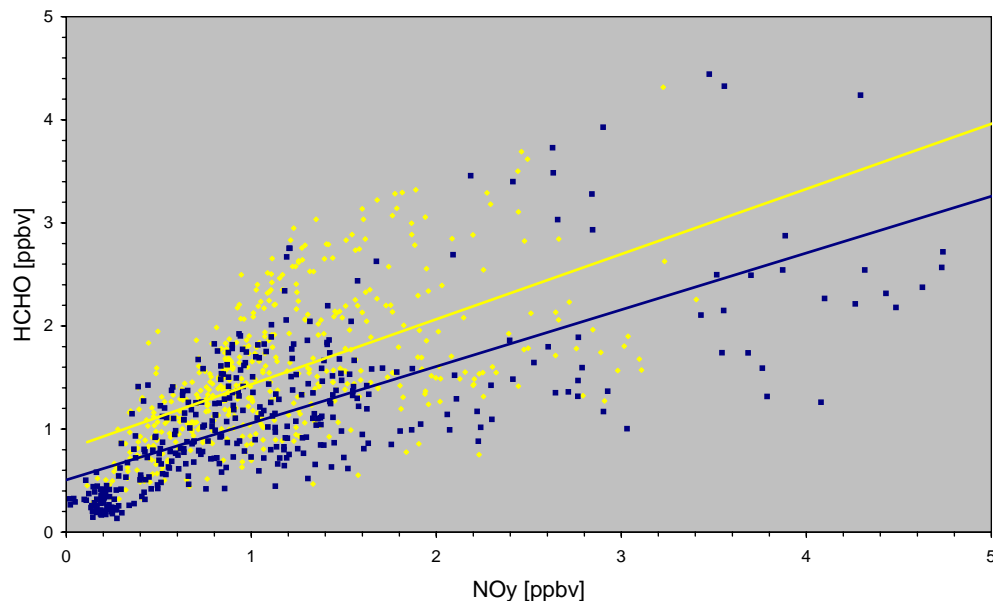
Fig. 6. Scatter plot of HCHO versus CO. Daytime data (06:00–20:00 GMT) are printed as yellow squares, while nighttime (20:00–06:00 GMT) observations are printed as dark blue diamonds. The individual regression lines for day and night are shown as yellow (HCHO = 0.026 CO - 1.85; $R^2 = 0.47$) and blue (HCHO = 0.035 CO - 3.14; $R^2 = 0.59$) lines, respectively. A linear regression analysis for the combined data yields: HCHO = 0.032 CO - 2.67; $R^2 = 0.54$.
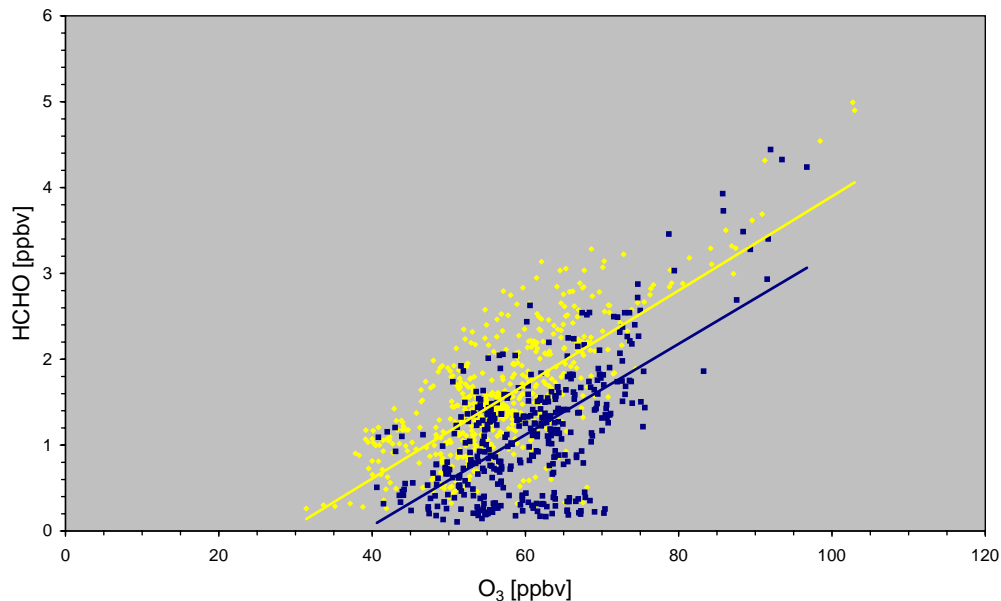
© EGU 2002

Fig. 7. Scatter plot of HCHO versus NO_y. Daytime data (06:00–20:00 GMT) are printed as yellow squares, while nighttime (20:00–06:00 GMT) observations are printed as dark blue diamonds. The individual regression lines for day and night are shown as yellow (HCHO = 0.63 NO_y + 0.8; R^2 = 0.35) and blue (HCHO = 0.55 NO_y + 0.5; R^2 = 0.51) lines, respectively. A linear regression analysis for the combined data yields: HCHO = 0.59 NO_y + 0.7; R^2 = 0.40.

Fig. 8. Scatter plot of HCHO versus O_3. Daytime data (06:00–20:00 GMT) are printed as yellow squares, while nighttime (20:00–06:00 GMT) observations are printed as dark blue diamonds. The individual regression lines for day and night are shown as yellow (HCHO = 0.055 O_3 - 1.57; R^2 = 0.55) and blue (HCHO = 0.051 O_3 - 1.95; R^2 = 0.41) lines, respectively. A linear regression analysis for the combined data yields: HCHO = 0.048 O_3 - 1.47; R^2 = 0.37.